ELSEVIER

Ceramics International 32 (2006) 499–507

CERAMICS INTERNATIONAL

www.elsevier.com/locate/ceramint

Unlubricated friction and wear behaviors of various alumina-based ceramic composites against cemented carbide

Deng Jianxin [a,*], Ding Zeliang [b], Zhao Jun [a], Li Jianfeng [a], Cao Tongkun [a]

[a] *Department of Mechanical Engineering, Shandong University, Jinan 250061, Shandong Province, PR China*
[b] *Department of Mechanical Engineering, Zhuzhou Polytechnic University, Zhuzhou 412008, Hunan Province, PR China*

Received 9 January 2004; received in revised form 25 May 2004; accepted 12 March 2005
Available online 1 June 2005

Abstract

Al_2O_3/TiC, Al_2O_3/Ti(C,N), Al_2O_3/(W,Ti)C, and Al_2O_3/SiC_w alumina-based composites, which provided a reasonably wide range of mechanical properties and microstructure, were produced by hot pressing. The unlubricated friction and wear behaviors of these composites against cemented carbide were studied in air atmosphere using the ring-block method. The friction coefficient and wear rates were measured, and the wear mechanisms were discussed in relation to mechanical properties and microstructure. Results showed that additions of TiC, Ti(C,N), (W,Ti)C, or SiC_w to the Al_2O_3 matrix increased the flexural strength, fracture toughness, and hardness compared to the monolithic Al_2O_3 matrix. The friction coefficient showed a downward trend with the increasing of the sliding speed, and decreased dramatically with increasing applied load for all the alumina-based composites. The Al_2O_3/TiC composite showed the highest wear rate, and the Al_2O_3/SiC_w the lowest one under identical test conditions. The higher wear resistance of Al_2O_3/SiC_w composite corresponded to its higher fracture toughness and hardness.

Keywords: C. Friction; D. Al_2O_3; Ceramics; Wear

1. Introduction

Ceramics have intrinsic characteristics, such as: high melting point, high hardness, good chemical inertness and high wear resistance, that make them promising candidates for wear resistance components, compared with metal alloys. Components made of advanced ceramics can survive and perform well, even improving their tribological properties. Nowadays advanced ceramics are widely used in cutting tools, dies for drawing or extrusion, seal rings, valve seats, bearing parts, and a variety of high temperature engine parts etc. [1–6].

However, the use of single-phase ceramics, even fully densified, in wear or structural applications are limited by the variability of their mechanical strength and poor fracture toughness. Their susceptibility to brittle fracture can lead to unexpected catastrophic failures. Improvement in mechanical properties must be achieved before the potential of these ceramics can be fully realized. Considerable improvement in mechanical properties of single-phase ceramics has been achieved by incorporating one or more other components into the base material to form ceramic-matrix composites (CMC) [7–10]. The reinforcing component is often in the shape of particles or whiskers. Ceramic composites with oxide matrices particularly Al_2O_3 are of increasing interest. Addition of hard particles or whiskers to the Al_2O_3 matrix may enhance its mechanical properties considerably. Some of these composites, e.g., Al_2O_3/TiC, Al_2O_3/Ti(C,N), Al_2O_3/(W,Ti)C, and Al_2O_3/SiC_w, have been used in various engineering applications and offer advantages with respect to friction and wear behaviors [1–3,11,12].

The increasing use of these alumina ceramic composites in a variety of applications in contact with themselves or other materials has engendered a need for understanding the tribological behavior of these materials. But there is little published information on the comparison of friction and wear behavior of these alumina based ceramic composites. In this paper, Al_2O_3/TiC, Al_2O_3/Ti(C,N), Al_2O_3/(W,Ti)C, and Al_2O_3/SiC_w alumina-based composites were produced

* Corresponding author.
E-mail address: jxdeng@sdu.edu.cn (D. Jianxin).

0272-8842/$30.00
doi:10.1016/j.ceramint.2005.03.031

to test further optimize their wear resistance. Particular attention was paid to the effect of mechanical properties and microstructure on the friction and wear behaviors of these composites against cemented carbide in air.

2. Materials and experimental procedures

2.1. Preparation of the ceramic materials

The starting powders were of commercial Al_2O_3 (average particle size 1.5 μm), TiC, Ti(C,N) and (W,Ti)C (average particle size 1.5 μm), and SiC whiskers (average diameter 1 μm, average aspect ratio 20). Alumina was used as the baseline material, additions of TiC, Ti(C,N), (W,Ti)C, or SiC whiskers were made to Al_2O_3 matrix according to the combinations listed in Table 1. The combined powders were prepared by wet ball milling in alcohol with cemented carbide balls. The material was fabricated using colloidal and ultrasonic processing techniques. Filter pressing was used to consolidate the multi-component slurries into green bodies approximately 60 mm in diameter and 15 mm thick. Following drying, the final densification of the compacted powder was done by the hot pressing sintering technique with a pressure of 35 MPa in argon atmosphere for 10–40 min to produce a ceramic disk. The required temperature are in the range of 1700–1900 °C. Details of the specific processing parameters employed are listed in Table 1.

Densities of the hot-pressed materials were measured by the Archimedes's method. Test pieces of 3 mm × 4 mm × 36 mm were prepared from the hot-pressed disks by cutting and grinding using a diamond wheel and were used for the measurement of flexural strength, Vickers hardness and fracture toughness. A three-point bending mode was used to measure the flexural strength over a 30 mm span at a crosshead speed of 0.5 mm/min. The Young modulus was calculated by measuring displacement in three-point bending. Vickers hardness was measured on polished surface of the specimens with a load of 98 N. The fracture toughness was determined by the indentation micro-fracture (IM) technique [13,14] with a load of 98 N using Eq. (1).

$$K_{IC} = 0.203\left(\frac{c}{a}\right)^{-3/2} Ha^{1/2} \quad (1)$$

where c is the radial crack length, a the impression half diagonal and H the hardness. The c and a were measured by the optical microscope. At least five number of indentations were made on each specimen. Data for flexural strength, Young modulus, hardness and fracture toughness of all the alumina-based composites were gathered on five specimens.

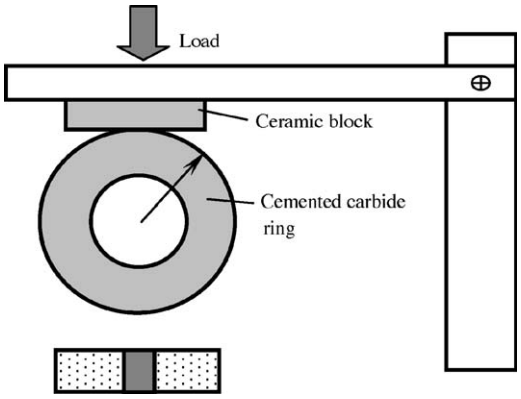

Fig. 1. Schematic diagram of the test apparatus.

2.2. Friction and wear tests

Friction and wear tests were conducted with a MRH-3 high-speed ring-block tribometer (made in China). The schematic diagram of this equipment is shown in Fig. 1. The block specimen (15 mm × 12 mm × 5 mm) was made of ceramic materials having a polished surface with a surface roughness of 0.08 μm. The ring specimen (∅ 50 mm × ∅ 35 mm × 15 mm) was made of cemented carbide (WC/Co) with a hardness of HRA 89 and was polished to produce a final surface roughness of 0.01 μm. Both the block and the ring were rinsed with hexane, then ultrasonically cleaned in fresh hexane, followed by ultrasonic cleaning with acetone. The surfaces perpendicular to the hot pressing direction of the Al_2O_3/SiC_w composite were chosen for the friction surface owing to the anisotropy in whisker distribution [15,16]. The ceramic block is fixed, while the cemented carbide ring is rotated with a speed of 100–550 rpm. A normal load of 30–150 N was added in all the tests. Each test was run over a period of 10 min. The friction coefficient was calculated by dividing the measured tangential force by the applied normal force. The mall loss of the worn ceramic blocks was measured with an accurate electron balance (minimum 0.001 mg). The wear rate W is defined as the volume loss, V, divided by the applied normal load, P, times the sliding distance, L.

$$W = \frac{V}{PL} \quad (2)$$

Table 1
Details of the specific processing parameters employed in hot-pressing processes

Specimen	Composition (vol.%)	Sintering temperature (°C)	Temperature holding time (min)	Hot pressing pressure (MPa)
Al_2O_3/TiC	Al_2O_3/55% TiC	1750	10–20	35.0
Al_2O_3/Ti(C,N)	Al_2O_3/30% Ti(C,N)	1750	10–20	35.0
Al_2O_3/(W,Ti)C	Al_2O_3/45% (W,Ti)C	1750	10–20	35.0
Al_2O_3/SiC_w	Al_2O_3/30% SiC_w	1850	20–40	35.0

where the W has the units of volume loss per unit force per unit distance (mm^3/N m).

The fracture surfaces and the worn regions of the ceramic blocks were examined using scanning electron microscopy (HITACH S-570).

3. Results and discussions

3.1. Mechanical properties and micro-structural characterization of the alumina-based ceramic composites

The materials used in the present investigation were of several hot-pressed alumina-based composites fabricated by the authors, which provided a reasonably wide range of mechanical properties and microstructure for the study. Results for flexural strength, fracture toughness, hardness, and density of these alumina-based composites are given in Table 2. Al_2O_3/TiC, Al_2O_3/Ti(C,N) and Al_2O_3/(Ti,W)C are particle-reinforced alumina-based composites, while Al_2O_3/SiC_w is a whisker reinforced composite. As expected, the additions of TiC, Ti(C,N), (W,Ti)C, or SiC_w to the Al_2O_3 matrix increased flexural strength, fracture toughness, and hardness compared to the monolithic Al_2O_3 matrix. In particular, the increase in fracture toughness (K_{IC}) for Al_2O_3/SiC_w composite was about 350% with respect to a monolithic Al_2O_3 matrix.

Fig. 2(a)–(c) shows the SEM micrographs of the fracture surface of Al_2O_3/TiC, Al_2O_3/Ti(C,N), and Al_2O_3/(W,Ti)C composites, respectively. From these micrographs, different morphologies can be clearly seen. These particle-reinforced composites exhibited a rough fracture surface and showed signs of longer crack deflection path, and the fracture mode was mixed transgranular and intergranular. Fig. 2(d) shows SEM micrograph of the fracture surface of Al_2O_3/SiC_w composite. Protruding whiskers and holes are an evidence of whisker pullout and bridging, which are the main toughening mechanisms of this composite.

Fig. 3(a)–(d) shows the SEM micrographs of the polished surfaces of Al_2O_3/TiC, Al_2O_3/Ti(C,N), Al_2O_3/(W,Ti)C, and Al_2O_3/SiC_w ceramic materials, respectively. Specimens were etched using a hot-solution of phosphoric acid. In Fig. 3(a)–(c) the white phases with clear contrast are of TiC Ti(C,N), or (W,Ti)C, and the grey phases are of Al_2O_3. Porosity is virtually absent, and the second phases are uniformly distributed within the matrix, and second-phase agglomeration or matrix segregation were absent in Al_2O_3/Ti(C,N)

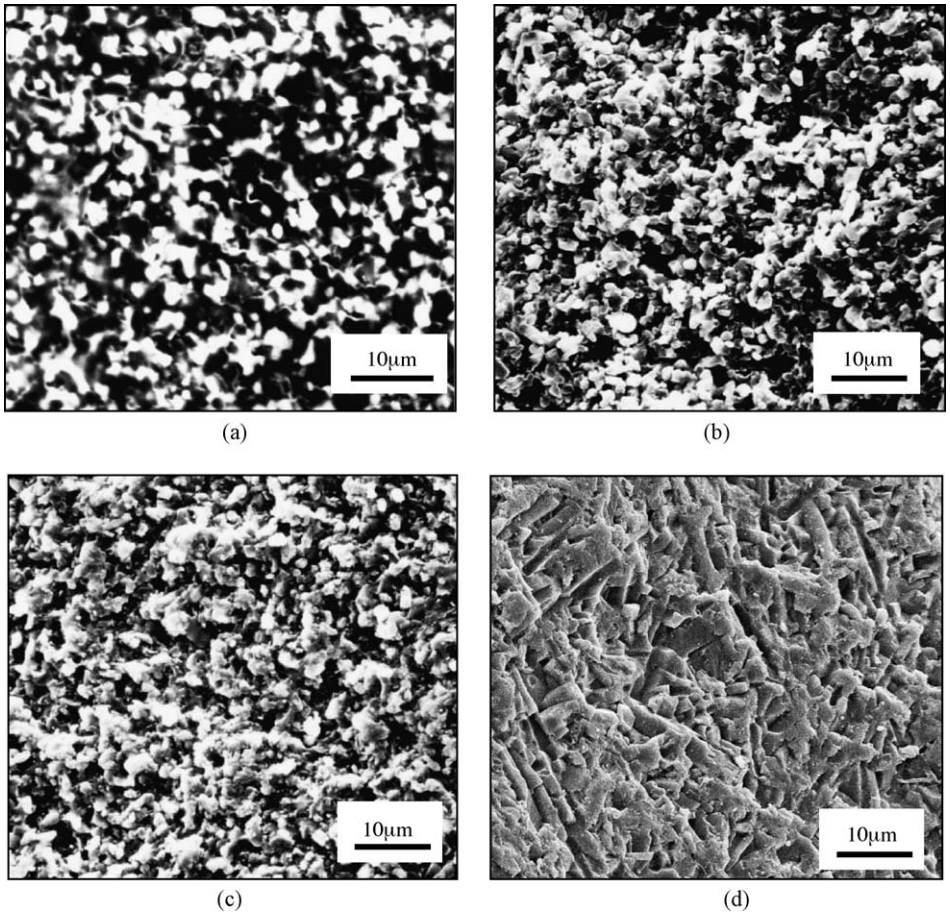

Fig. 2. SEM micrographs of the fracture surfaces of (a) Al_2O_3/TiC, (b) Al_2O_3/Ti(C,N), (c) Al_2O_3/(W,Ti)C, and (d) Al_2O_3/SiC_w composites.

Table 2
The composition and mechanical properties of alumina-based composites

Sample	Density (g/cm^3)	Flexural strength (MPa)	Fracture toughness, K_{IC} (MPa m$^{1/2}$)	Hardness, H_V (GPa)	Young modulus, E (GPa)
Al_2O_3	3.92	300–400	2.5	19.0	380
Al_2O_3/TiC	4.90	900–1000	4.5	20.5	420
Al_2O_3/Ti(C,N)	4.55	700–900	4.9	21.0	410
Al_2O_3/(W,Ti)C	6.64	800–900	5.2	21.5	430
Al_2O_3/SiC_w	3.66	700–850	8.5	22.5	400

and Al_2O_3/(W,Ti)C. The Al_2O_3/TiC composite showed a growth and agglomeration of smaller grains, and Al_2O_3/(W,Ti)C composite exhibited the smallest grain size (less than 1 μm). Fig. 3(d) shows the optical micrograph of the polished surfaces perpendicular to the hot pressing direction of Al_2O_3/SiC_w composites, where the white needle-like phases are SiC whiskers.

3.2. Friction and wear behaviors of the alumina-based ceramic composites

The effect of the applied load and sliding speed on the friction coefficient of all the ceramic blocks are shown in Fig. 4. The friction coefficient showed a downward trend with the increase of the sliding speed, and was the lower, the higher the applied load for all the tested composites. The Al_2O_3/(W,Ti)C ceramic composite exhibited the smallest, and the Al_2O_3/SiC_w composite the highest friction coefficient under the same test conditions.

Fig. 5 shows the cumulative volume loss of the ceramic blocks with the sliding distance and the applied load. It can be seen that the cumulative volume loss continuously increased with the sliding distance for all the tested specimens. The Al_2O_3/SiC_w composite showed the smallest volume loss, while the Al_2O_3/TiC composite exhibited the highest volume loss at the same test conditions. The higher the applied load, the higher the volume loss of the ceramic blocks.

Fig. 6(a) shows the SEM micrograph of the worn surface of the Al_2O_3/TiC composite, which reveals the existence of a considerable number of pits and craters. The SEM micrograph of the worn surface at higher magnification is shown in Fig. 6(b). A significant surface damage with smeared, deformed appearance can be observed on the wear

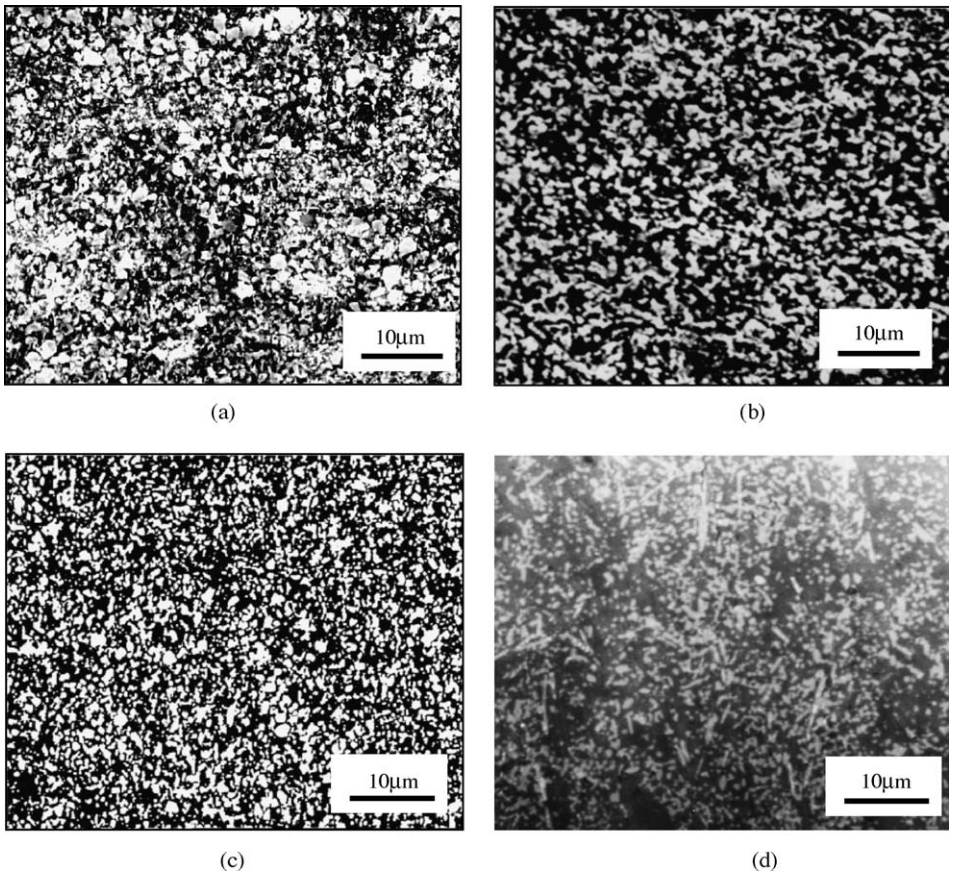

Fig. 3. SEM micrographs of the polished surfaces of (a) Al_2O_3/TiC, (b) Al_2O_3/Ti(C,N), (c) Al_2O_3/(W,Ti)C, and (d) Al_2O_3/SiC_w composites.

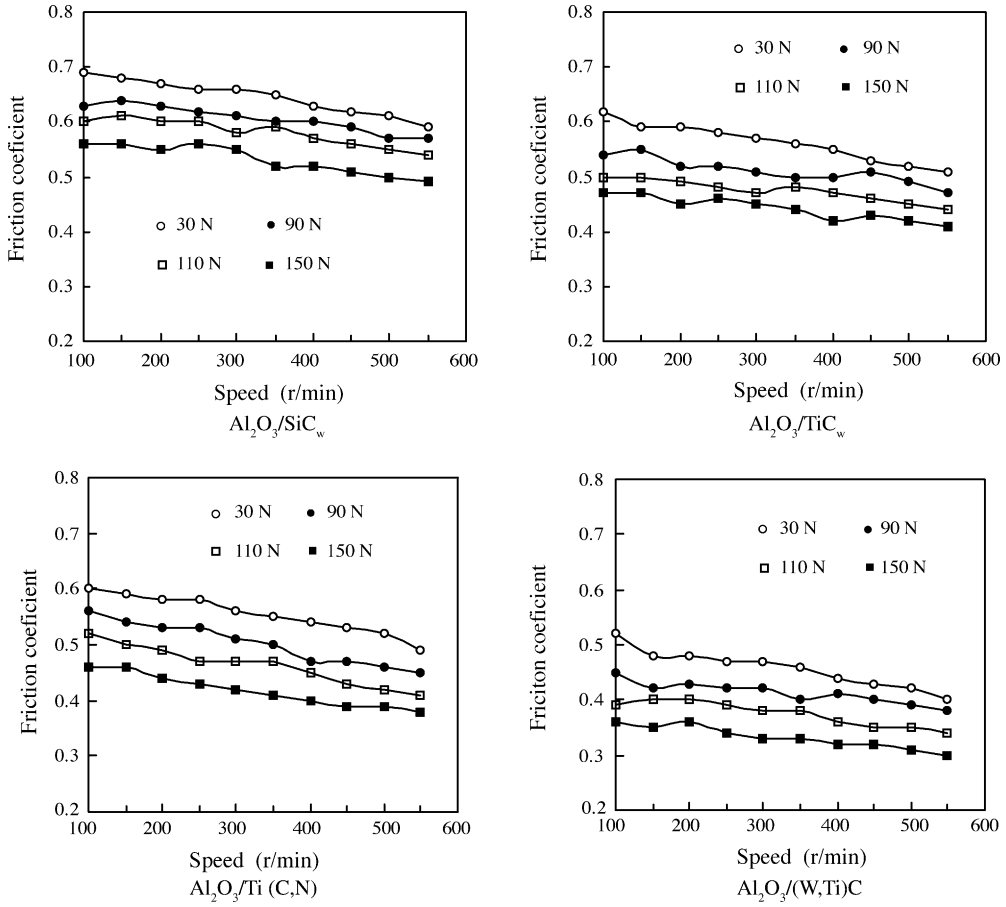

Fig. 4. Effect of the applied load and sliding speed on the friction coefficient for all the ceramic composites.

track. There are a lot of micro-cracks located on the worn surface indicating that brittle fracture took place.

Typical SEM micrographs of the worn surfaces of Al_2O_3/Ti(C,N) composite are shown in Fig. 7. The wear track was mangled, and showed a brushing off of debris on the worn surface. Fig. 8 shows SEM micrographs of the worn surfaces of Al_2O_3/(W,Ti)C composite. There were numerous pits and scratches on the wear surface. This suggests that the primary wear mechanism under these conditions is brittle fracture.

A typical SEM micrograph of the wear track of the whisker-reinforced composite (Al_2O_3/SiC_w) is shown in Fig. 9. The deep micro-grooves on the worn surface indicate whisker debonding and removal. Since the friction surfaces perpendicular to the hot pressing direction were chosen for that composite, many whiskers lie on the friction surface, and could bridge sub-surface cracks. Such cracks, propagating through the matrix, are responsible for whisker debonding [17,18].

Several studies [19,20] have shown that indentation cracks formation in ceramics may result from elas-plastic fracture. This type of fracture is characterized firstly by plastic deformation of the contact area, with subsurface lateral cracks propagating outward from the base of the contact zone on planes nearly parallel to the surface, and with median cracks propagating from the contact zone normal to the surface. Debris removal is thought to occur primarily by surface chipping, when lateral cracks curve up and intersect the surface, while median cracks remain in the surface and influence strength subsequently. Since the formation and propagation of the lateral and median cracks are closely related to the properties of the composites, wear rates are expected to depend on mechanical properties and microstructure.

The most important parameters that control the debris removal are identified by indentation fracture mechanics. The lateral crack C_L length and the mean depth h are given by [19,20]

$$C_L \propto \left[\left(\frac{E}{H_V}^{3/4}\right) K_{IC}^{-1} H_V^{-1/4}\right]^{1/2} P^{5/8} \quad (3)$$

$$h \propto \left(\frac{E}{H_V}\right)^{1/2} \left(\frac{P}{H_V}\right)^{1/2} \quad (4)$$

where E and H_V are elastic modulus and the Vicker's hardness of the materials, and P is the mean vertical force. It can be seen from Eqs. (2) and (3) that the size of the lateral and median crack grows with a decrease in fracture toughness and an increase of the load.

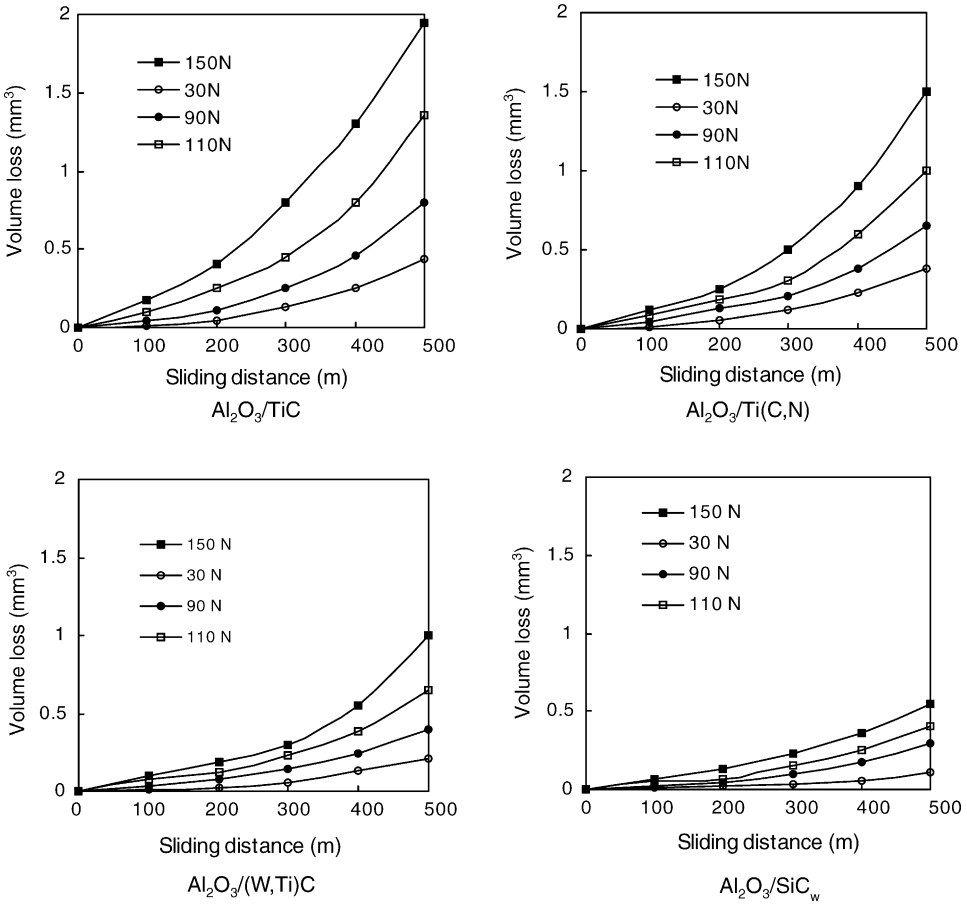

Fig. 5. The cumulative volume loss of the ceramic blocks with sliding distance and the applied load.

Assuming the volume removed by a grit (indentor) under a normal load P_i to be proportional to the dimensions of the lateral crack length C_L and the mean depth h, the volume removal V_i for one grit is obtained as [21]:

$$V_i \propto \alpha_i \frac{P_i^{9/8}}{K_{IC}^{1/2} H_V^{5/8}} \left(\frac{E}{H_V}\right)^{4/5} \quad (5)$$

where α_i is a materials independent constant. Therefore, the total volumetric removal V with a normal load P and the mechanical properties would follow an equation of the form

$$V \propto \alpha \frac{P^{9/8}}{K_{IC}^{1/2} H_V^{5/8}} \left(\frac{E}{H_V}\right)^{4/5} \quad (6)$$

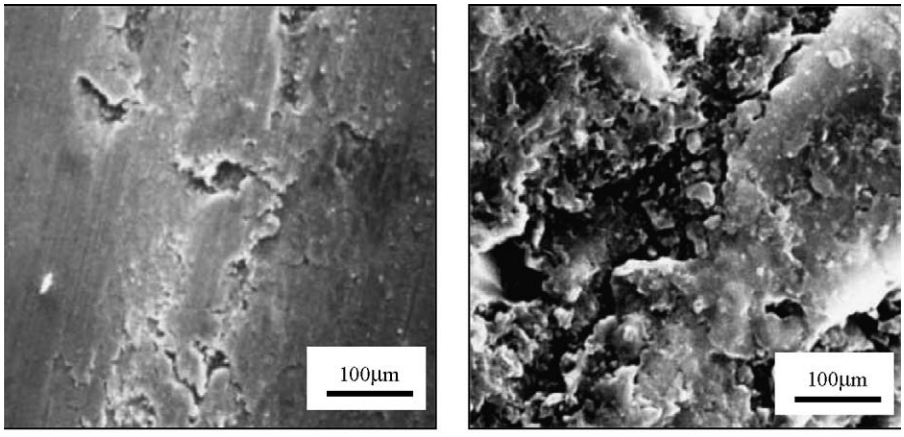

Fig. 6. SEM micrographs of the worn surfaces of the Al_2O_3/TiC composite.

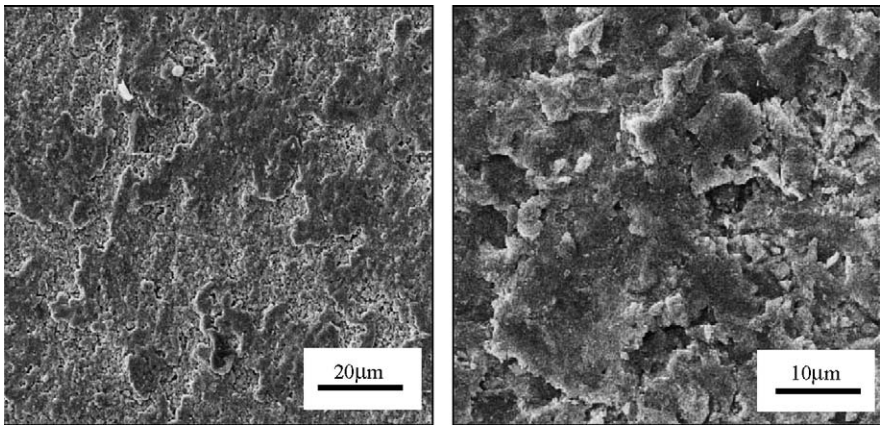

Fig. 7. SEM micrographs of the worn surfaces of the Al_2O_3/Ti(C,N) composite.

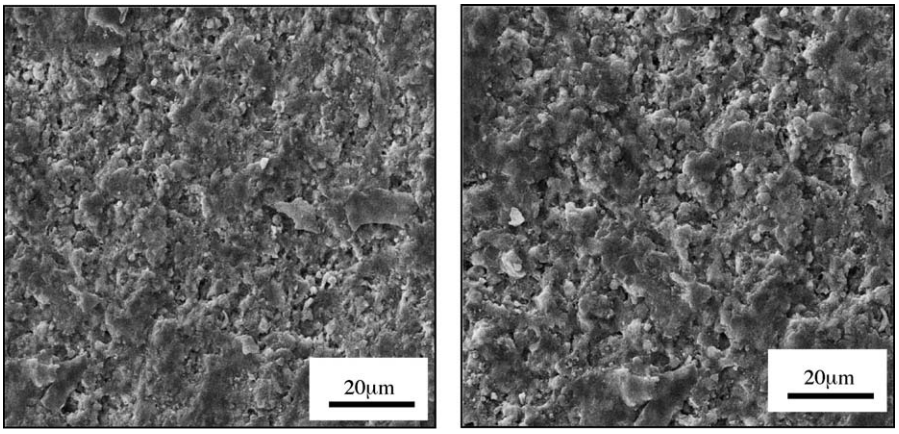

Fig. 8. SEM micrographs of the worn surfaces of the Al_2O_3/(W,Ti)C composite.

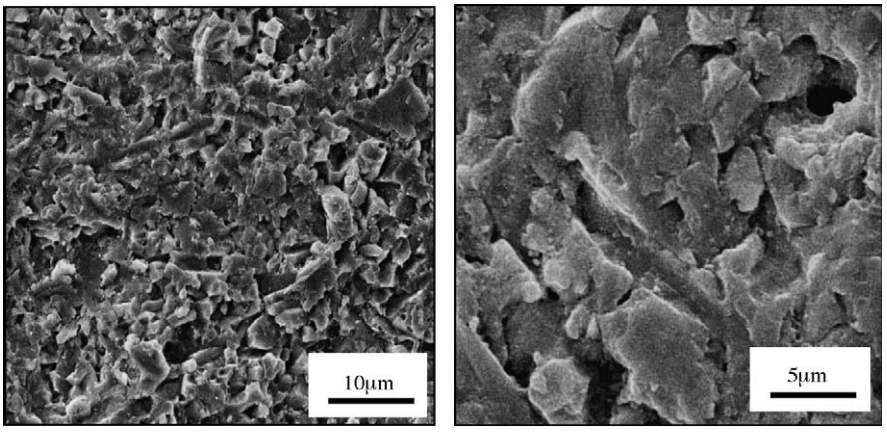

Fig. 9. SEM micrographs of the worn surfaces of Al_2O_3/SiC_w composite.

Thus, Eq. (2) could be written

$$W = \frac{V}{PL} \propto \alpha \frac{P^{1/8}}{K_{IC}^{1/2} H_V^{5/8} L} \left(\frac{E}{H_V} \right)^{4/5} \quad (7)$$

In Fig. 10 the wear rate of different alumina-based composites is plotted logarithmically as a function of the applied load (P). It can be seen from these results that as the applied load increases, there is an increase in wear rates. A linear relationship between the logarithmic values of the wear rate and the applied load was observed. The measured slopes of the corresponding regression lines are 0.1973, 0.1575, 0.1348, and 0.0868 for Al_2O_3/TiC, Al_2O_3/Ti(C,N), Al_2O_3/(W,Ti)C, and Al_2O_3/SiC_w composites, respectively, while the exponents of P in Eq. (7) is 0.125. It seems that the applied load has greater influence on the

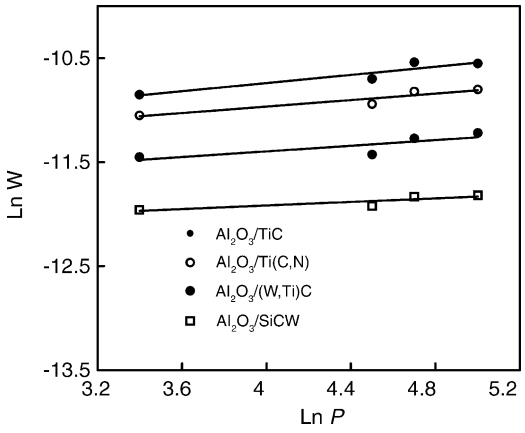

Fig. 10. Logarithmically plot of wear rates vs. the applied load for different alumina-based composites (operation time: 10 min).

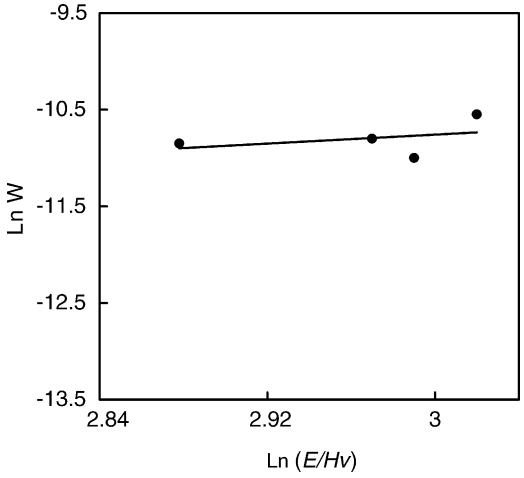

Fig. 12. Logarithmically plot of wear rates vs. the ratio of E/H_V (applied load: 150 N).

wear rates for the composites with lower fracture toughness and hardness.

The logarithmically variation in wear rate with the fracture toughness (K_{IC}) for different alumina-based composites under the same test conditions is shown in Fig. 11. It can be seen that the K_{IC} played an important role on the wear rate. The composites with higher K_{IC} showed the smaller wear rate. The measured slope of the corresponding regression line is -1.815, while the exponent of K_{IC} in Eq. (7) is only -0.5. It seems that Eq. (7) underestimate the dependence on K_{IC}. The reason could be that the sliding surface is already weakened by median cracks from previous contact. In other words, the effective H_V of the material could be itself K_{IC} dependent.

In Fig. 12 the wear rate is plotted logarithmically with the ratio of E/H_V for different alumina-based composites under identical test conditions. It can be seen from these results that the composites with lower ratio of E/H_V showed the smaller wear rate. The measured slope of the corresponding regression line is 1.1638, while the exponent of E/H_V in Eq. (7) is 0.8. There is almost a linear relationship between the logarithmic values of the wear rate and the ratio of E/H_V.

The results confirm that the wear resistance of the alumina-based composites tested not only depends on the applied load, but also depends on their mechanical properties. The observation is in agreement with that of Eq. (7). The composites with high fracture toughness and hardness exhibited lower wear rates and better wear resistance. The higher wear resistance of the whisker-reinforced alumina composite corresponded to its higher values of hardness and fracture toughness.

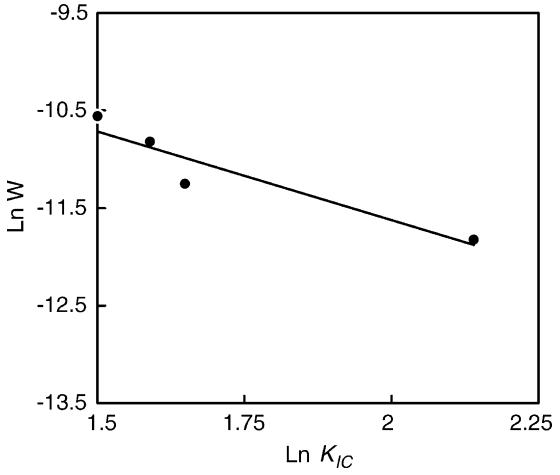

Fig. 11. Logarithmically plot of wear rates vs. the fracture toughness K_{IC} (applied load: 150 N).

4. Conclusions

Al_2O_3/TiC, Al_2O_3/Ti(C,N), Al_2O_3/(W,Ti)C, and Al_2O_3/SiC_w alumina-based composites were produced to further optimise its wear resistance. Particular attention was paid to the effect of mechanical properties and microstructure on the friction and wear behaviors of these composites. Results showed that:

1. Additions of TiC, Ti(C,N), (W,Ti)C, or SiC_w to the Al_2O_3 matrix increased the flexural strength, fracture toughness, and hardness compared to the monolithic Al_2O_3 matrix.
2. The friction coefficient showed a downward trend with the increasing of the sliding speed, and decreased dramatically when with higher applied load for all the alumina-based composites. The Al_2O_3/(W,Ti)C composite exhibited the smallest friction coefficient, and the Al_2O_3/SiC_w composite the highest under the identical test conditions.
3. The Al_2O_3/SiC_w composite showed the smallest wear rate, while the Al_2O_3/TiC composite the highest. The applied load, fracture toughness and ratio of E/H_V played an important role with respect to the wear rate. The higher wear resistance of Al_2O_3/SiC_w composite corresponded to its higher fracture toughness and hardness.

Acknowledgement

This work was supported by ''the National Natural Science Foundation of China (50275088, 50475133)'', ''the Excellent Young Teachers Program of MOE (2055)'', and ''the Scientific Research Foundation for the Excellent Young Scientists of Shandong Province (02BS064)''.

References

[1] B. John, J.R. Wachtman, Structural Ceramics, Academic Press, Inc., London, 1989.
[2] D.W. Richerson, Modern Ceramic Engineering, Marcel Dekker, Inc., New York, 1992.
[3] A. Xing, L. Zhaoqian, D. Jianxin, Development and perspective of advanced ceramic cutting tool materials, Key Eng. Mater. 108 (1995) 53–66.
[4] S. Jahanmir, Tribological applications for advanced ceramics, Mater. Res. Soc. Symp. Proc., Materials Research Society Publication 140 (1989) 285–291.
[5] D.C. Cerammer, Ceramic tribology needs and opportunities, Tribol. Trans. 31 (2) (1987) 164–171.
[6] S. Jahanmir, Friction and wear of ceramics, Tribol. Int. 28 (6) (1995) 421–427.
[7] A.G. Evans, Perspective on the development of high toughness ceramics, J. Am. Ceram. Soc. 73 (2) (1990) 187–195.
[8] R.W. Steinbrech, Toughening mechanisms for ceramic materials, J. Eur. Ceram. Soc. 8 (10) (1992) 131–137.
[9] P.F. Becher, Microstructural design of toughened ceramics, J. Am. Ceram. Soc. 74 (2) (1991) 255–269.
[10] E.D. Whitney, Microstructural engineering of ceramic cutting tools, Ceram. Bull. 67 (6) (1988) 1010–1015.
[11] D. Jianxin, A. Xing, Friction and wear behavior of Al_2O_3/TiB_2 composite against cemented carbide in various atmospheres at elevated temperature, Wear 195 (1996) 128–132.
[12] G. Brandt, Ceramic cutting tools, state of the art and development trends, Mater. Technol. 14 (1) (1999) 17–22.
[13] R.F. Cook, B.R. Lawn, A modified indentation toughness technique, J. Am. Ceram. Soc. 66 (11) (1983) C200–C201.
[14] K. Niihara, A. Nakahira, T. Hirai, The effect of stoichiometry on mechanical properties of boron carbide, J. Am. Ceram. Soc. 67 (1) (1984) C13–C14.
[15] J. Vigneau, P. Bordel, Influence of the microstructure of the composite ceramic tools on their performance when machining nickel alloys, Ann. CIRP 36 (1987) 13–16.
[16] F. Lee, M.S. Sandlin, Toughness anisotropy in textured ceramics, J. Am. Ceram. Soc. 76 (6) (1993) 1793–1800.
[17] Lee Taichiu, Jianxin Deng, Ultrasonic erosion of whisker reinforced ceramic composites, Ceram. Int. 27 (7) (2001) 755–760.
[18] Deng Jianxin, Ai Xing, Effect of whisker orientation on the friction and wear behavior of $Al_2O_3/TiB_2/SiC_w$ composites in sliding wear tests and in machining processes, Wear 201 (1996) 178–185.
[19] D.B. Marshall, B.R. Lawn, A.G. Evans, Elastic/plastic indentation damage in ceramics: the lateral crack system, J. Am. Ceram. Soc. 65 (11) (1982) 561–566.
[20] B.R. Lawn, A.G. Evans, D.B. Marshall, Elastic/plastic indentation damage in ceramics: the median/radial crack system, J. Am. Ceram. Soc. 63 (9–10) (1980) 574–581.
[21] A.G. Evans, D.B. Marshall, in: D.A. Rigney (Ed.), Fundamental of friction and wear of materials, ASME, 1981, p. 439.